ASR AND ITS MITIGATION IN MORTARS CONTAINING RECYCLED SODA-LIME GLASS AGGREGATES

Farshad Rajabipour*, Hamed Maraghechi, Seyed M.H. Shafaatian

The Pennsylvania State University, University Park, PA, USA
* Corresponding author: farshad@psu.edu

Abstract

This paper summarizes a study to better understand the mechanisms and mitigation of ASR caused by recycled glass aggregates. Glass particles exhibit an unusual size-effect in which their reactivity lessens by reducing the particle size in the range 2.36 to 0.1mm. SEM reveals that contrary to the common assumption, the surface of glass does not undergo ASR. Rather, ASR initiates inside intra-particle cracks which are originated during bottle crushing. When these cracks are healed by annealing or when crack-free glass beads with same composition are used, mortars pass the innocuous threshold of ASTM C1260. SEM image analysis shows that smaller glass particles contain tighter cracks (i.e., less permeable) and smaller number of cracks which may explain why they are less reactive. The study further investigates how fly ash mitigates ASR in ASTM C1567 mortars. The results show that transport reduction and alkali binding are the most dominant mitigation mechanisms.

Keywords: Recycled glass, intra-particle cracks, ASR mitigation, ion transport, alkali binding

1 INTRODUCTION

The practice of recycling glass containers and windows is growing in many countries. Unfortunately, a significant portion (~600,000 tons/year in the United States [1,2]) of the collected glass is not actually recycled into new glass; mainly due to prohibitive shipping costs from collection points to glass melting facilities. One alternative application for glass cullet is as aggregate in construction materials. The incentive is to divert waste from landfills and to find a local material source to reduce the need for quarrying and transportation of natural aggregates. For example, research [3,4,5] has shown that concrete with desirable workability and strength can be produced, by using recycled glass as fine aggregates. However, the alkali-silica reaction (ASR) must be mitigated. This paper presents a summary of research aimed at understanding the mechanism of ASR and its mitigation in concrete materials containing crushed soda-lime glass aggregates. The paper includes two main sections. First, the mechanism of ASR induced by recycled glass is reviewed. Second, experimental work is presented to assess how fly ash mitigates ASR in the accelerated mortar bar test (ASTM C1567) containing recycled glass sand. While the important findings are included in this summary paper, the reader is referred to [6,7,8] for further description of experimental methods and discussions.

2 MECHANISM OF ASR FOR SODA-LIME GLASS SAND

Previous research [3,9,10] has focused on relating the severity of ASR expansions to the size, content, and color of glass aggregates. In particular, it was found that expansions and cracking generally decrease by reducing the particle size of glass [3]. Figure 1(a) provides an example in which mortars containing a combination of recycled glass sand and natural glacier sand were tested for ASR expansion per ASTM C1260 [11]. Recycled glass made up 0% to 50% of the total sand on a weight basis. The results show that

expansions tend to decrease by reducing the average size of glass particles. While a pessimum average size of 1.8 mm (associated with glass particles between #8 and #16 sieves) is observed, finer particles show significantly smaller expansions.

This size-dependent trend of glass reactivity is counter-intuitive when ASR is considered a surface reaction which should accelerate by increasing the surface area of reactive aggregates. This behavior is seldom observed with natural reactive aggregates unless the aggregate is ground to a very fine size (<100μm), resulting in a pozzolanic reaction instead of ASR [12,13]. A number of hypotheses have been offered to explain this unusual size-effect trend. Bazant and Steffens [14] suggested that the swelling pressure of ASR gel strongly depends on the aggregate size and is maximum at some intermediate particle size. Bazant et. al. [15] further suggested that while the chemical reactions of ASR could accelerate by reducing the particle size, the stress intensity factor is simultaneously and non-linearly reduced, favoring less cracking for smaller aggregates. Suwito et al. [16] hypothesized that smaller aggregates result in a larger volume of porous ITZ, which provides space for free expansion of ASR gel without exerting swelling stresses. These hypotheses are all based on the assumption that ASR occurs at the glass-cement paste interface. This assumption was later shown to be incorrect by SEM imaging, as discussed in the next paragraph. In addition, it has been argued that fine glass powder has pozzolanic properties [4,17], which can mitigate the ASR of larger particles. However, the pozzolanic reaction of glass was shown to be significant only for very fine particles (< 38μm) [18]. Such fine particles are absent in ASTM C1260 tests that resulted in expansions shown in Figure 1(a).

Our recent work [6] based on SEM imaging of mortar bars during ASTM C1260 test revealed that for soda-lime glass, ASR occurs within microcracks in the interior of glass particles and not at the glass-cement paste interface. Figure 2(a) shows formation of ASR gel in the interior of a glass particle, while the glass-paste interface has largely remained intact. Several other SEM images of different magnifications are provided in [6,11]; all confirming the same conclusions. Similar observations were made in SEM images of concrete prisms after 1 year exposure in ASTM C1293 test.

In addition, it was found that at least some of these microcracks originate during bottle crushing and are pre-existing before glass is used in concrete. Figure 2(b) shows a SEM image of a glass particle that was epoxy impregnated immediately after crushing. Despite no exposure to cement paste or alkalis, microcracks exist inside glass particle. These microcracks are filled with epoxy, verifying that they were formed during bottle crushing and not during SEM sample preparation.

To further evaluate the hypothesis that "Recycled soda-lime glass undergoes ASR only within intra-particle microcracks", two additional experiments were performed. In the first experiment, crushed glass cullet was annealed at different temperatures in the range 560-680^{o}C. Annealing softens glass which results in viscous healing of microcracks. The driving force is the surface energy of glass at crack faces which results in viscous flow of glass under capillary forces near a crack tip. Figure 3 shows healing of a star-shape set of cracks made by micro-indentation of a glass microscope slide. As the temperature is increased inside a hot-stage ESEM, cracks start to heal from the two tips and can completely disappear after few minutes depending on the viscosity (temperature dependent) of glass.

In Figure 1(b), the results of ASTM C1260 test on mortar bars made with annealed or non-annealed glass cullet is reported. Details of the annealing procedure are included in [7]. It is observed that annealing reduces ASR expansions and glass cullet annealed at 650^{o}C for 40 minutes can be considered innocuous based on ASTM C1260. SEM images of mortar cross sections after 14 days of NaOH bath exposure show little to no sign of ASR gel or cracking for mortars made with properly annealed glass cullet.

In the second experiment, ASTM C1260 mortar bars were prepared using spherical soda-lime glass beads (3 mm diameter) as fine aggregates with volume fraction 46%. The beads have similar oxide composition as glass cullet but are not crushed and do not contain intra-particle cracks. Little expansion was

observed in these mortars even after 4 weeks of NaOH exposure (Figure 4(a)). For comparison, the expansion of mortar bars containing 46% vol. crushed cullet in the narrow size range 4.75 to 2.36 mm (#4 to #8 sieves) (Avg. = 3.6 mm) is also shown. Figure 4(b) shows SEM micrograph of glass bead mortar after 12 weeks of NaOH exposure. No sign of damage or ASR gel is observed. However, a non-expansive C-S-H gel has formed at the glass-cement paste interface as a result of a pozzolanic reaction at high temperature and alkali concentrations. Both conditions favor dissolution of glass bead and the resulting silicate ions react with available portlandite at the surface of glass (e.g., see Figure 2(a)) to form C-S-H. Table 1 shows the oxide compositions of glass, ASR gel, and pozzolanic C-S-H which are obtained by X-ray EDS. Each data point is the average of at least 5 EDS spot measurements in Figures 2(a) and 4(b).

To evaluate the extent and size of the microcracks induced by bottle crushing, SEM imaging was performed on crushed glass particles of three different size fractions: 1.18~2.36 mm (#8~#16 mesh), 0.3~0.6 mm (#30~#50 mesh), and 0.075~0.15 mm (#100~#200 mesh). Image analysis of 10 representative micrographs from each size fraction showed that smaller glass particles contain tighter cracks and a smaller number of cracks [7]. This may explain why smaller glass particles are less reactive. Their tighter microcracks mitigate water permeation and diffusion of OH^- and alkali ions to the interior of glass which are required for formation and swelling of the ASR gel.

3 HOW DOES FLY ASH MITIGATE ASR IN ASTM C1567 TEST?

The first half of this paper described how soda-lime glass cullet undergoes ASR inside concrete, and illustrated the significance of residual microcracks in determining the reactivity of glass aggregates. In the second half, the focus is shifted to gaining a better understanding of ASR mitigation by fly ash in materials containing glass aggregates. Specifically, we like to examine why fly ash reduces ASR in the accelerated mortar bar test (ASTM C1567) and to a lesser extent, how the effectiveness of fly ash is related to its composition.

Previous studies [19,20,21] on concrete containing natural reactive aggregates suggested that by alkali dilution and binding, fly ash reduces the pH of pore solution and mitigates ASR. Replacement of cement with fly ash may dilute the alkali content of pore solution since fly ash alkalis dissolve very slowly comparing to alkalis from Portland cement [19]. The additional pozzolanic C-S-H binds some alkalis and removes them from pore solution. A lower C/S and incorporation of alumina (originating from fly ash) also improve the alkali binding capacity of pozzolanic C-S-H [22,23]. Thomas [22] showed a strong correlation between the pore fluid alkalinity and concrete prism expansions in ASTM C1293 test. In addition to alkali dilution/binding, pozzolanic reactions can, over time, reduce the mass transport and increase the tensile strength of concrete [24,25]. Transport reduction is especially significant where an external source of alkalis is present (e.g., deicing salts); while strength improvement aids in resisting internal stresses and cracking. Finally, use of fly ash could alter the composition of ASR gel (e.g., reduce its CaO/Na_2O_{eq}), which may reduce its viscosity and swelling capacity [26,27]. Bleszynski and Thomas [28] reported massive formation of ASR gel in ASTM C1567 mortars containing reactive flint and fly ash. However, presumably due to its low viscosity, this gel diffused freely in cement paste without exerting damage.

Fly ash has been shown to mitigate ASR in both long-term and accelerated tests. While the mitigation mechanisms (alkali dilution, binding, transport, strength, gel modification) has been well documented for ASTM C1293 [22], their contributions during ASTM C1567 test are still a matter of debate. For example:

(a) Doesn't submersion of mortar bars in an inexhaustible bath of alkalis (1N NaOH) neutralize the benefits of alkali dilution and binding?
(b) Can fly ash reduce transport and improve strength of mortars during the course of ASTM C1567 test (when mortars are less than 16 days old)?
(c) Is fly ash stopping ASR or merely delaying it in this test?

To start addressing these questions, specifically for mortars containing recycled glass sand, 6 different fly ashes were studied including 4 class F and 2 class C ashes. ASTM C1567 test was performed on mortars containing 100% recycled glass sand and various replacement levels of Portland cement with any of these 6 ashes. Figure 5(a) reports the 14day expansion results. All ashes reduced ASR expansions but, as anticipated, they are not equally effective. The minimum dosage of each fly ash necessary to reduce expansions below a 0.1% threshold was determined as: 15%F1, 15%F2, 20%F3, 20%F4, 25%C1 and 35%C2.

The oxide compositions of the cement and fly ashes are shown in the ternary phase diagram of Figure 5(b) (oxide contents were normalized by subtracting the values for SO_3 and LOI). It is evident that fly ashes with higher CaO_{eq} contents are less effective in mitigating ASR. The phase diagram also shows the oxide contents of composite binders that were able to mitigate ASR (e.g., 85%PC+15%F1, etc.). Remarkably, all composite binders are clustered in one area of the diagram below a CaO_{eq} value of 61%. It would be interesting to test other combinations of different cements and fly ashes to determine if a maximum CaO_{eq} can be identified to ensure controlling of ASR in mortars containing glass sand. Similar threshold values might be established for other reactive aggregates. Of course, other fly ash properties such as its particle size and glass content affect its efficiency. In this work, the 6 fly ashes had comparable particle size distributions as quantified by laser diffraction.

To evaluate the contribution of the five ASR mitigation mechanisms discussed above, a set of experiments were performed on ASTM C1567 mortars: tensile and compressive strength, porosity, transport properties, pore fluid extraction and analysis, and microstructural analysis by SEM/EDS. Also, a numerical simulation was performed to model the penetration of alkalis from soak solution and their binding by C-S-H. For details of experiments and numerical model, see [8]. A summary of the results is provided below.

3.1 Tensile and Compressive Strength

The strength results are shown in Figure 6 where the tensile and compressive strength of the control mortar (100% cement) is compared with mortars containing the required dose of fly ash to mitigate ASR. The tensile strength (modulus of rupture) was measured by 3-point bending of mortar prisms (25×25×250 mm). For each mixture, 4 prisms were tested and the results averaged. The error bars in Figure 6 represent ±1 standard deviation. The compressive strength was measured on mortar cubes (50×50×50 mm) per ASTM C109. For each mixture, 3 cubes were tested and the results averaged. Both tests were performed on specimens after 3 days exposure to NaOH bath at 80°C. This age was selected since microcracking and ASR expansion was observed to initiate in the control mortar after 3 days. Prior to NaOH exposure, the specimens were moist cured for 24h and then submerged in tap water at 80°C for 24h (ASTM C1567).

The mortars containing fly ash show higher tensile (13% to 38%) and compressive (0% to 54%) strength values in comparison with the control mortar. This is contrary to a common observation of lower early-age strength when cement is replaced with fly ash at regular service temperatures. The higher strengths in this test are potentially caused by high temperature and high alkali exposure of mortars which accelerate the pozzolanic reaction of fly ash. In parallel, the porosity of binder phase was measured (per ASTM C127) by preparing 100%PC and PC-fly ash pastes of similar proportions and curing. The results at 3d NaOH exposure were 40.1%, 43.8%, and 46.2% for the control, 15%F_1, and 35%C_2 binders. This suggests that strength improvement was not due to reduction in porosity and may have been caused by other factors such as modified pore size distribution or increase in aggregate-paste bond strength.

3.2 Ion Diffusion Coefficient

The ion diffusivity of mortars was measured non-destructively through application of the Nernst-Einstein equation [29]:

$$\frac{\sigma}{\sigma_0} = \frac{D}{D_0} = \varphi\beta = \frac{1}{F} \quad (1)$$

This method has been frequently used for evaluating the transport properties of cementitious and other porous materials [30]. The resistance of a porous microstructure to transport of ions is quantified in terms of its "formation factor" F which is proportional to the ratio of diffusion coefficient of an ion in pore solution, D_o (m^2/s), to the effective diffusion coefficient of that ion in the mortar. According to Eq. (1), F is inversely proportional to the product of porosity φ (-), and pore connectivity β (-) and can be determined by independent measurements of the electrical conductivity of material and conductivity of pore solution. In this study, electrical conductivity of mortar bars were measured by connecting two embedded stainless steel electrodes to an electrical impedance analyzer. In parallel, the pore fluid of mortars was extracted at specific ages and its conductivity measured using a commercial solution conductivity meter. The results are presented in Figure 7(a) which compares the diffusivity of the control, 15%F_1, and 35%C_2 mortars over the duration of ASTM C1567 test.

The findings strongly suggest transport reduction as a dominant ASR mitigation mechanism by fly ash in this test. The diffusivity of the control mortar is higher than the fly ash mortars by a factor of 3 to 7. This means that alkali and OH^- ions can travel much faster into the control mortar. This is confirmed by pore solution analysis data described below. For the control mortar, diffusivity increases from 0 to 3 and 7 days but subsequently decreases. The initial increase is probably due to microcracking caused by ASR. As these cracks are filled by ASR gel (with much lower electrical conductivity than pore solution), the overall conductivity and diffusivity of the mortar decrease. The diffusivity of the fly ash mortars remains relatively constant during the test period.

3.3 Pore Solution Analysis

Pore solutions were extracted at the following ages after casting: 0d, 1d (demolding), 2d (after 24h 80°C-water bath), 5d, 9d, 16d (the last 3 correspond to 3d, 7d, 14d exposure to NaOH bath). The extracted solutions were analyzed by HCl titration for $[OH^-]$ measurement and ICP-AES for determining the concentrations of Na, K, Ca, Si, S and Al elements. Figure 7(b) shows $[OH^-]$ over the duration of ASTM C1567 test (the results for other elements are included in [8]). At 0d, all 3 mortars have $[OH^-] \approx 100$mM. During the first 24 hours, concentrations rise mainly due to cement hydration. At 24h, $[OH^-]$ of fly ash mortars is 22% and 34% less than the control mortar; which shows the effect of alkali dilution. During the next 24 hours, mortars are submerged in a water bath which promotes leaching of alkalis. The rate of leaching is proportional to the ion diffusivity of mortars and is the highest for 100%PC. At 48h, the $[OH^-]$ has dropped to 170 to 270mM and the effect of alkali dilution is nearly totally erased. During the next 14 days, $[OH^-]$ of mortar pore solutions increase steadily due to exposure to NaOH bath. The control mortar shows the highest concentrations which agrees with its high diffusion coefficient. The dissolution rate of glass is strongly related to the pH [31]; which justifies the highest rate of ASR in 100%PC mortar. These observations further underline the importance of ion transport as a major mechanism of ASR mitigation during ASTM C1567 test. It should be noted that at 16d, the rate of increase in $[OH^-]$ for fly ash mortars is similar or higher than the control mortar. This may suggest that fly ash mortars will eventually undergo ASR as $[OH^-]$ reaches higher values.

3.4 Microstructural Analysis by SEM/EDS

SEM/EDS imaging was performed on control and fly ash mortars at 9d and 16d. The goal was to address two main questions. (1) Does ASR gel form in large quantities in fly ash mortars? (2) Does the use of fly ash alter the composition of ASR gel? Figure 8(a) shows representative images from the 15%F_1 mortar.

While the control mortar was severely distressed by ASR, only minor traces of ASR gel is detected in the fly ash mortar. In other words, the presence of fly ash has prevented the dissolution of glass aggregates. The results of EDS compositional analysis of ASR gels (Table 2) show similar compositions between the control and fly ash mortars. Also no significant variation in the gel composition was observed from the surface to the interior of mortar prisms or in gels from mortars after 7 or 14 days of NaOH exposure.

3.5 Numerical Model to Simulate Alkali Transport and Binding

A 1D finite-difference model was developed to simulate diffusion of NaOH from the soak solution by solving Fick's 2nd law. Ion diffusion was simulated across a mortar cross section of 25×25mm^2 that is exposed to 1N NaOH from two opposite faces (1D model). The other two faces were considered as sealed. Mortar diffusion coefficients were obtained from Figure 7(a) (0d values were used). Diffusivity of NaOH in pore solution (D_o) at 80°C was used as 2.343×10^{-9} m^2/s [32], ignoring the effect of ion activity coefficients. The model included a sink term to account for alkali binding by C-S-H according to distribution ratio [23]:

$$R_d = \frac{\text{[Na] in solid C-S-H (Mol/kg)}}{\text{[Na] in pore solution (Mol/Lit)}} \quad (2)$$

The values of R_d used in the model were a function of Ca/Si of C-S-H according to the work of Hong and Glasser [23]. For 100%PC mortar (Ca/Si=1.87), R_d=0.5; and for 15%F_1 mortar (Ca/Si=1.39), R_d=1.25 were used. Ca/Si was determined by EDS of C-S-H phase in 100%PC and 15%F_1 pastes (average of 10 spots was used). The pore solution was assumed to only contain Na and OH ions; as such multi-ion diffusion was ignored. At every point within the pore solution, charge neutrality was maintained meaning: $[Na^+]=[OH^-]$. Initial condition was defined as $[OH^-]=0.23$M across the thickness of mortar for both control and fly ash mortars (corresponding to average 2d value in Figure 7(b)). Boundary condition was $[OH^-]=1.0$M at 0 and 25mm. Further model details are included in [8].

Figure 8(b) shows the results. The triangles and squares show simulated $[OH^-]$ profiles corresponding to the control and 15%F_1 mortars. The fly ash mortar shows lower concentrations due to a combination of lower ion diffusivity and higher C-S-H binding capacity. The two middle curves quantify the contributions of lower diffusivity and higher binding individually. The circles show how improving the C-S-H binding capacity while maintaining the same diffusion coefficient results in lower $[OH^-]$. The diamonds show the opposite case suggesting that reducing ion diffusivity while maintaining the binding capacity leads to even lower $[OH^-]$. Overall, both transport reduction and alkali binding seem to be significant in delaying the increase in pore solution's pH.

4 CONCLUSIONS

- The residual cracks in the interior of crushed recycled glass aggregates are responsible for their alkali-silica reactivity. In the absence of these cracks (e.g., in glass beads or annealed glass cullet), ASR is minimal or non-existent. Larger glass particles are more reactive since they contain wider cracks (more permeable) and higher crack density.
- The principal mechanisms of ASR mitigation by fly ash in ASTM C1567 test are reducing ion diffusivity and improving the alkali binding capacity of C-S-H. In addition, fly ash mortars exhibited higher tensile and compressive strength as little as 3 days after exposure to NaOH.

REFERENCES

[1] J. Reindl, Reuse/recycling of glass cullet for non-container uses, www.glassonline.com/infoserv/Glass_recycle_reuse/Glass_reuse_recycling_doc1.pdf, Accessed Jul. 15, 2011.

[2] U.S. Environmental Protection Agency (EPA), Washington, DC, "Municipal solid waste generation, recycling, and disposal in the United States: Facts and figures for 2009". 2010.

[3] W. Jin, C. Meyer, S. Baxter, Glascrete - Concrete with glass aggregate, ACI Mat J, 2000, 97(2), 208-213.
[4] A. Shayan, A.M. Xu, Value-added utilisation of waste glass in concrete, Cem Con Res, 2004, 34(1), 81-89.
[5] C. Polley, S.M. Cramer, R.V. de la Cruz, Potential for using waste glass in portland cement concrete, ASCE J of Materials, 1998, 10(4), 210-219.
[6] F. Rajabipour, H. Maraghechi, G. Fischer, Investigating the alkali-silica reaction of recycled glass aggregates in concrete materials, ASCE J of Materials, 2010, 22(12), 1201-1208.
[7] H. Maraghechi, S. Shafaatian, G. Fischer, F. Rajabipour, The role of residual cracks on alkali silica reactivity of recycled glass aggregates, Cem Con Comp, 2012, 34(1), 41-47
[8] S. Shafaatian, A. Akhavan, H. Maraghechi, F. Rajabipour, Study of the mechanisms of ASR mitigation by fly ash in ASTM C1567 mortars containing recycled glass aggregates, Cem Con Res, In review
[9] P.K. Mukherjee, J.A. Bickley, Performance of glass as concrete aggregates, 7th ICAAR, Ottawa, Canada, 1986, P. 36-42.
[10] H.Y. Zhu, E.A. Byars, Alkali-silica reaction of recycled glass in concrete, 12th ICAAR, Beijing, China, 2004, 811-820
[11] H. Maraghechi, Utilization of recycled glass as sand or cement replacement in concrete materials, MSc thesis, U of Hawai'i, 2010.
[12] T.E. Stanton, Expansion of concrete through reaction between cement and aggregate, Proc. of the ASCE, 1940, 66, 1781-1811.
[13] H.E. Vivian, The effect on mortar expansion of particle size of the reactive component in aggregate, Australian J of Applied Science, 1951, 2, 488-492
[14] Z.P. Bazant, A. Steffens, Mathematical model for kinetics of alkali-silica reaction in concrete, Cem Con Res, 2000, 30(3), 419-428
[15] Z.P. Bazant, G. Zi, C. Meyer, Fracture mechanics of ASR in concretes with waste glass particles of different sizes, ASCE J of Eng Mech, 2000, 126(3), 226-232.
[16] A. Suwito, W. Jin, Y. Xi, C. Meyer, A mathematical model for the pessimum size effect of ASR in concrete, Con Sci Eng, 2002, 4(13), 23-34.
[17] N. Schwarz, N. Neithalath, Influence of fine glass powder on cement hydration: Comparison to fly ash and modeling the degree of hydration, Cem Con Res, 2008, 38(4), 429-436.
[18] Y. Shao, T. Lefort, S. Moras, D. Rodriguez, Studies on concrete containing ground waste glass, Cem Con Res, 2000, 30(1), 91-100.
[19] S. Diamond, Effects of two Danish fly ashes on alkali contents of pore solutions of cement-fly ash pastes, Cem Con Res, 1981, 11(3), 383-394.
[20] D.W. Hobbs, Influence of pulverized-fuel ash and granulated blast furnace slag upon expansion caused by the alkali-silica reaction, Mag of Con Res, 1982, 34(1), 83-94.
[21] J. Duchesne, M.A. Bérubé, The effectiveness of supplementary cementing materials in suppressing expansion due to ASR; II: Pore solution chemistry, Cem Con Res, 1994, 24(8), 1579-1581.
[22] M.D.A. Thomas, The effect of supplementary cementing materials on alkali-silica reaction, Cem Con Res, 2011, 41, 209-216
[23] S.Y. Hong, F.P. Glasser, Alkali binding in cement pastes: Part I. The C-S-H phase, Cem Con Res, 1999, 32(7), 1893-1903
[24] R.N. Swamy, The Alkali-Silica Reaction in Concrete, Routledge, 1992
[25] B. Lothenbach, K.Scrivener, R.D. Hooton, Supplementary cementitious materials, Cem Con Res, 2011, 41, 217–229
[26] P.J.M. Monteiro, K. Wang, G. Sposito, M.C. dos Santos, W.P. de Andrade, Influence of mineral admixtures on the alkali-aggregate reaction, Cem Con Res, 1997, 27(12), 1899-1909.
[27] A. Bonakdar, B. Mobasher, S.K. Dey, D.M. Roy, Correlation of reaction products and expansion potential in alkali-silica reaction for blended cement materials, ACI Mat J, 2010, 107(4), 380-386.
[28] R.F. Bleszynski, M.D.A. Thomas, Microstructural studies of alkali-silica reaction in fly ash concrete immersed in alkaline solutions, Adv Cem Based Mat, 1998, 7(2), 66-78.
[29] A. Atkinson, A.K. Nickerson, The diffusion of ions through water-saturated cement, J of Mat Sci, 1984, 19(9), 3068-3078
[30] F.A.L. Dullien, Porous media: Fluid transport and pore structure, Academic Press, New York, 1979
[31] R.K. Iler, Chemistry of silica - Solubility, polymerization, colloid and surface properties and biochemistry, 1979, Wiley, New York
[32] CRC Handbook of chemistry and physics, 90th Ed., CRC Press, Boca Raton, Florida, 2010

Table 1: Average EDS oxide compositions for unreacted soda-lime glass, ASR gel, and pozzolanic C-S-H

Material	**SiO_2 (%)**	**CaO (%)**	**Na_2O (%)**	**SiO_2/CaO**
Soda-lime glass	74.0	14.0	9.6	5.29
ASR gel	64.1	19.9	13.1	3.22
Pozzolanic C-S-H	43.8	43.4	5.2	1.01

Table 2: Average atomic composition (wt.%) of ASR gel measured by EDS (at 14d NaOH exposure)

	Na	**Ca**	**Si**	**K**	**Al**	**Mg**	**Ca/Si**
Control	10.63	6.73	22.39	0.31	0.77	0.36	0.30
15%F1	7.24	5.50	24.89	0.64	0.73	0.37	0.22
35%C2	9.28	5.86	23.42	1.02	0.65	0.37	0.25

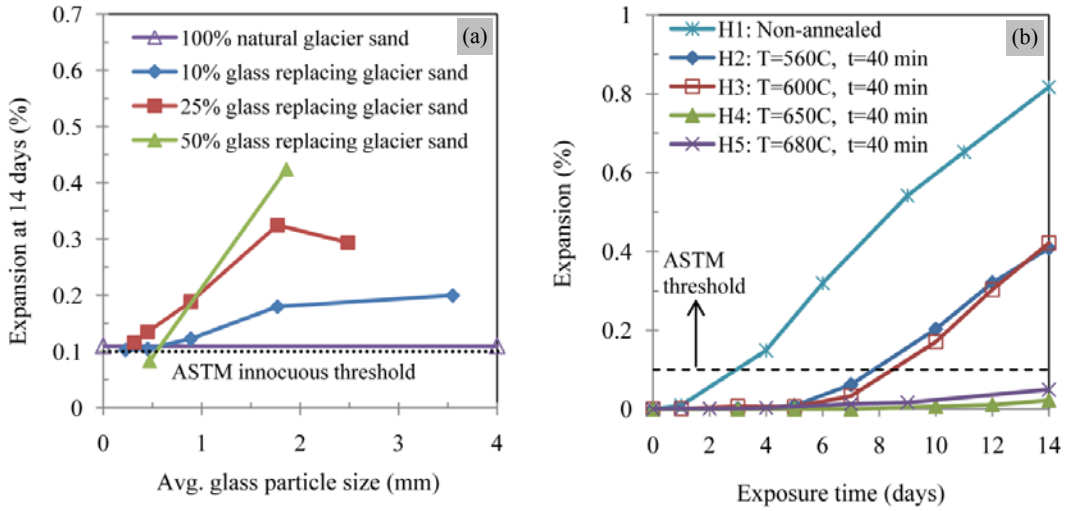

Figure 1: (a) Dependence of ASR expansion on the glass sand particle size in ASTM C1260 test; (b) ASR expansion of mortars made with glass sand annealed at different temperatures

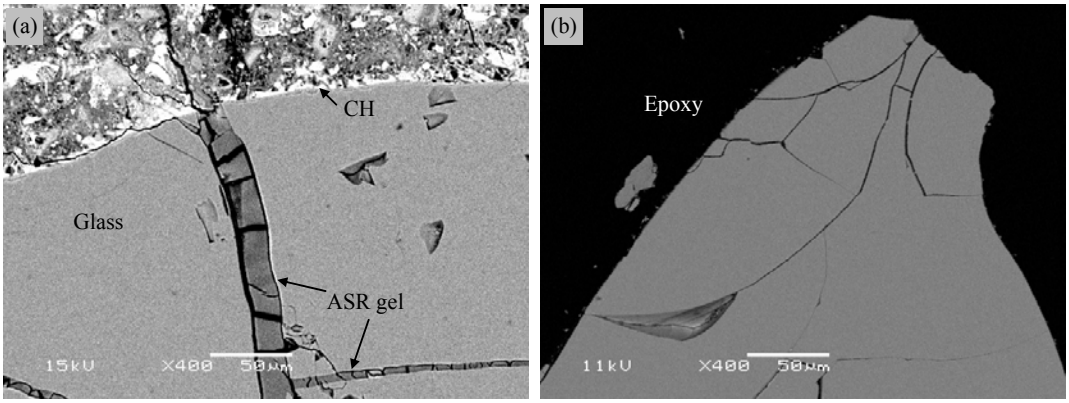

Figure 2: (a) ASR affected glass particle (size: 1.18~2.36mm) showing intra-particle gel formation in mortar after 14 days in ASTM C1260 test; (b) Pre-existing microcracks in glass particles induced by bottle crushing

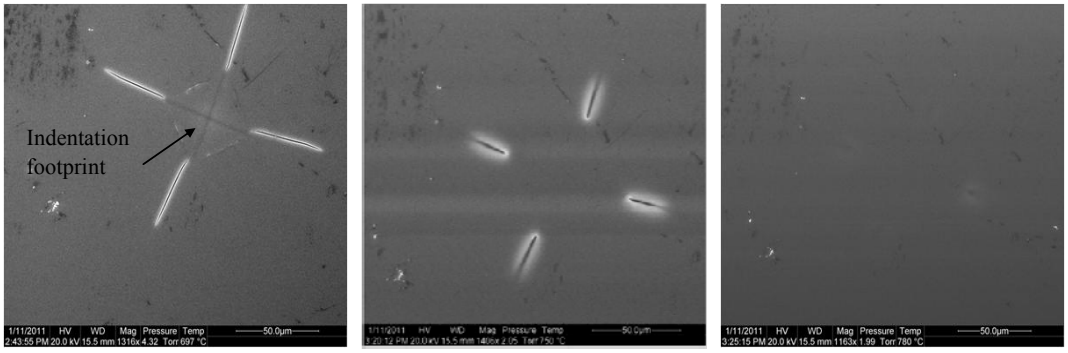

Figure 3: Viscous healing of microcracks in a soda-lime glass slide inside a hot stage ESEM

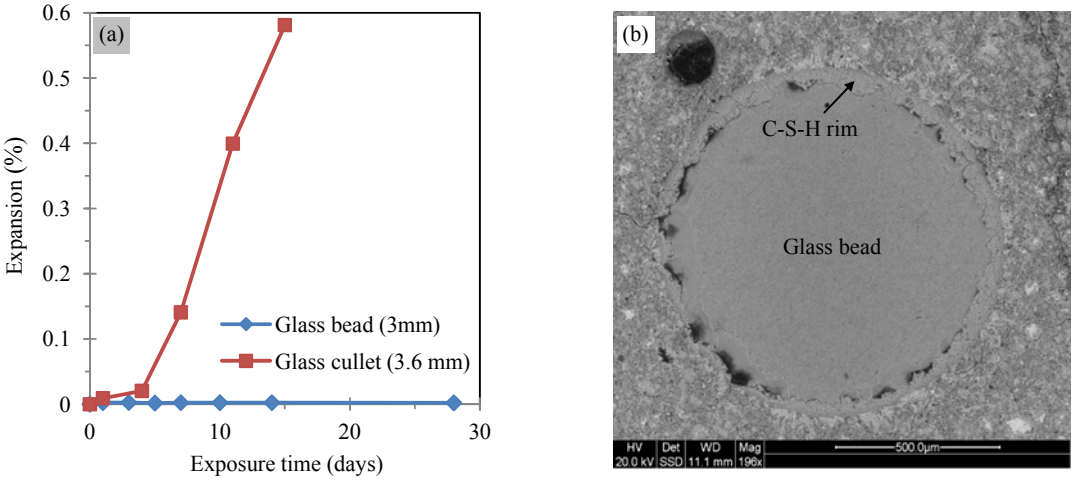

Figure 4: (a) ASTM C1260 expansions in mortars containing mono-size glass bead or glass cullet aggregates, (b) SEM image of glass bead in mortar after 12 weeks NaOH exposure

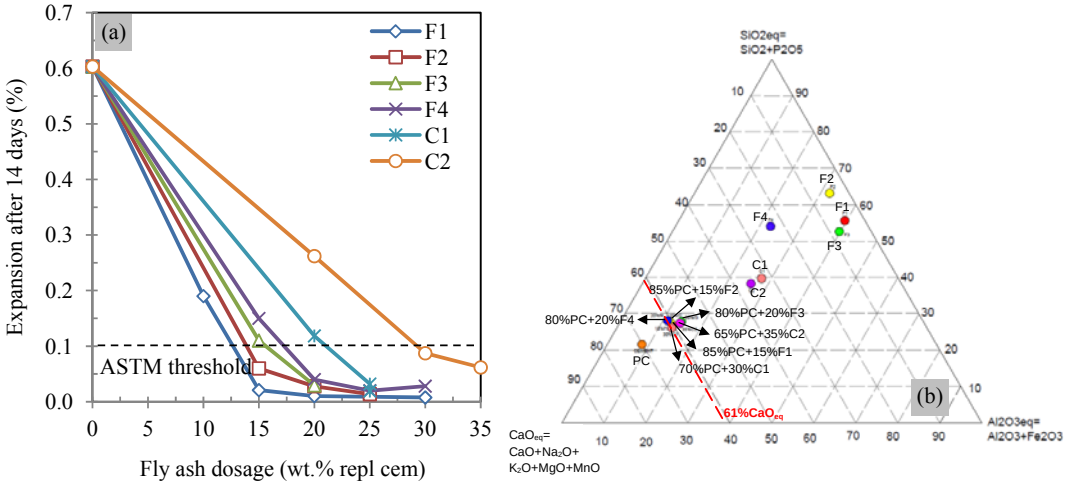

Figure 5: (a) ASTM C1567 expansion results as a function of fly ash type and dosage; (b) Ternary phase diagram showing compositions of cement, fly ashes, and composite binders

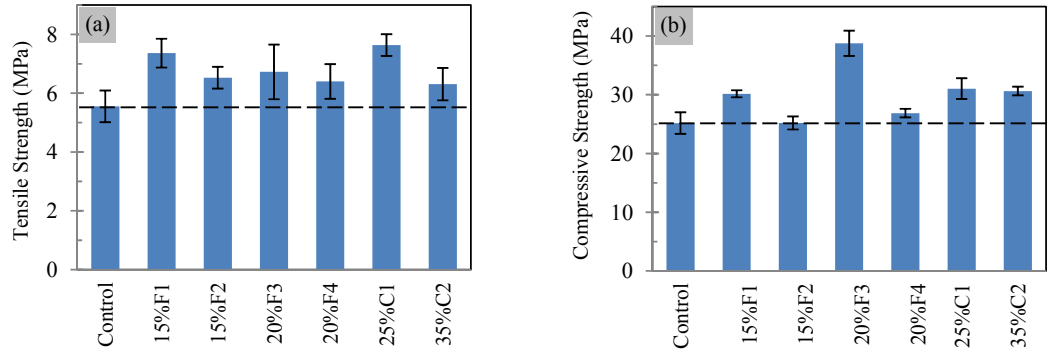

Figure 6: The tensile (a) and compressive (b) strengths of the control mortar and those containing fly ash

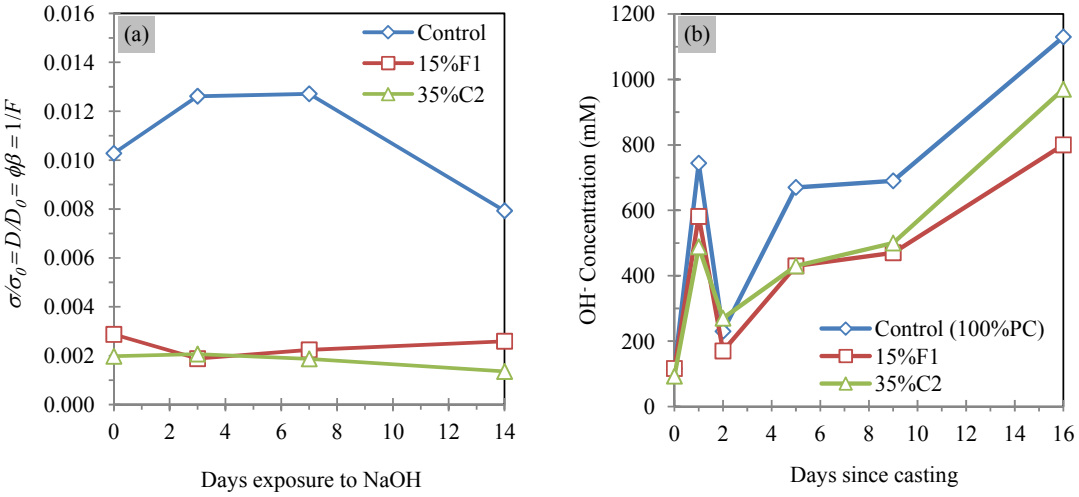

Figure 7: (a) Ion diffusivity and (b) Pore solution's [OH-] of the control and fly ash mortars during ASTM C1567 test

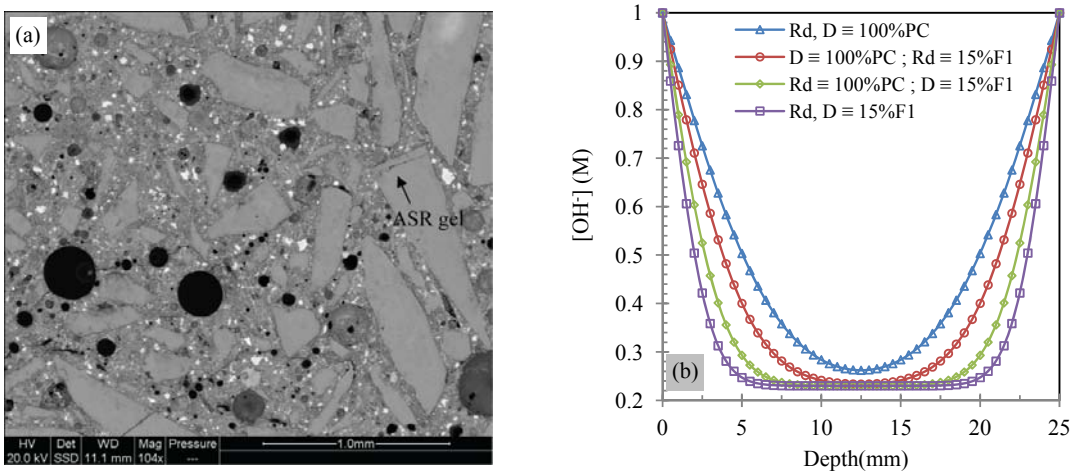

Figure 8: (a) SEM image of 15%F_1 mortar at 16d; (b) Simulation results showing the contributions of ion diffusion and binding